

Immobilization of Iron Oxide Magnetic Nanoparticles for Enhancement of Vessel Wall Magnetic Resonance Imaging—An *Ex Vivo* Feasibility Study

Binh Thai Nguyen,^{†,‡} Praveen Kumar Vemula,^{†,‡,§,||} Dimitrios Mitsouras,[⊥] Peng Yu,[#] Ming Tao,[#] Christina Campagna,[#] Robert V. Mulkern,[⊥] Frank J. Rybicki,[⊥] Jeffrey M. Karp,^{*,§,||} and C. Keith Ozaki^{*,#}

Department of Medicine, Brigham and Women's Hospital, Harvard Medical School, Harvard-MIT Division of Health Sciences & Technology, 65 Landsdowne Street, Cambridge, Massachusetts 02139, Harvard Stem Cell Institute, Harvard Medical School, and Applied Imaging Science Laboratory, Department of Radiology, and Department of Surgery, Brigham and Women's Hospital, Harvard Medical School, 75 Francis Street, Boston, Massachusetts 02115. Received March 15, 2010;

Revised Manuscript Received June 1, 2010

Emerging data supports a role for negative wall remodeling in the failure of vascular interventions such as vein grafts, yet clinicians/researchers currently lack the ability to temporally/efficiently investigate adventitial surface topography/total vascular wall anatomy *in vivo*. We established a strategy of immobilizing commercially available iron oxide magnetic nanoparticles (Fe-NPs) onto the surface of human vein conduits to facilitate high-throughput total vascular wall demarcation with magnetic resonance (MR). Binding of activated Fe-NPs to amine groups on the surface of the veins induced a thin layer of negative contrast that differentiated the adventitia from surrounding saline signal in all MR images, enabling delineation of total wall anatomy; this was not possible in simultaneously imaged unlabeled control veins. Under the conditions of this *ex vivo* experiment, stable covalent binding of Fe-NPs can be achieved (dose-dependent) on human vein surface for MR detection, suggesting a potential strategy for enhancing the ability of MRI to investigate total wall adaptation and remodeling in vein graft failure.

Over half a million vein grafts are implanted in the United States each year, and yet the task of maintaining vein graft patency continues to represent a major challenge for cardiac and vascular clinicians. Almost 40% of lower extremity vein bypass grafts develop occlusive lesions or fail within a year (1), and almost half of cardiac bypass patients will lose (>75% stenosis) a vein graft within the first year (2). This manifests as significant morbidity and mortality for patients and contributes to the enormous cost of cardiovascular health care related expenses. For decades, researchers have sought to understand the clinical, biological, and hemodynamic factors that contribute to neointimal hyperplasia, the presumed primary pathophysiology for early (1–18 months postimplantation) vein graft failure. Vein wall thickening and neointimal hyperplasia develop as an adaptive response to the arterial environment; luminal loss seen directly with angiography, or indirectly as increased velocity detected by duplex sonography, has traditionally been viewed as a pathological dysregulation of this process. However, with the increasing recognition of entire vessel wall negative vein graft remodeling as a significant contributor to vein graft failure (3–6), there exists an opportunity and need for advances in vascular imaging techniques to study total vein graft wall adaptations and remodeling.

Magnetic resonance imaging (MRI) is a powerful noninvasive diagnostic technique and a well-validated modality for vessel wall (and surrounding soft tissue) imaging (7). However, it is

limited to modest spatial resolutions (e.g., $0.4 \times 0.4 \times 4 \text{ mm}^3$) that, while adequate to study atherosclerosis in medium to large arteries, are largely inadequate for small-caliber vessels such as human vein grafts (8). Even achieving such comparatively high (by MR standards) spatial resolution poses a further limitation with respect to attainable craniocaudal coverage. For example, at clinical 1.5–3 T MRI magnetic field strengths, a 10 min scan suffices to image a 3–12 cm portion of a vessel (8–10). Lower resolutions require less imaging time and can enable increased coverage, but accurate delineation of the anatomy of the tissue interfaces becomes increasingly difficult to achieve due to partial voluming of the different tissues (i.e., one voxel containing multiple tissues presents a signal intensity that is the average of those of the underlying tissues).

One approach to overcome these challenges would be to coat vein grafts with an implantable contrast agent at the time of original surgical placement that can be readily identified by MRI, thereby facilitating efficient longitudinal imaging of the vessel wall with reduced reliance on imaging resolution. Vein grafts are often present on the operating room back table for up to thirty minutes, a time that has been utilized for other graft wall modifications (1). Superparamagnetic magnetic nanoparticles (Fe-NPs) have been widely used as ultrasensitive negative contrast agents for a wide range of applications such as stem cell tracking and early detection of cancers (11–13). Over the past decade, Fe-NPs have been explored for biomedical applications such as molecular imaging of cardiovascular disease, gene delivery, magnetic drug targeting, nanomedicine, and regenerative medicine (14, 15). These Fe-NPs provide an attractive alternative to other commercially available contrast agents because they are nontoxic and biocompatible, can undergo selective magnetization only when exposed to a magnetic field, and also allow a targetable delivery with particle localization in a specific area (16). Utilizing these advantages, we have developed a method to attach Fe-NPs on the surface of human veins, that can be performed under physiological

* Corresponding authors. Jeffrey M. Karp, Ph.D., Tel: 617-817 9174, Fax: 617-768-8338, E-mail: jkarp@rics.bwh.harvard.edu. C. Keith Ozaki, M.D., Tel: 857-307-1920, Fax: 857-307-1922, E-mail: CKOzaki@partners.org.

[†] Authors contributed equally.

[‡] Kauffman Foundation Entrepreneur Postdoc Fellow.

[§] Harvard-MIT Division of Health Sciences & Technology.

^{||} Harvard Stem Cell Institute.

[⊥] Department of Radiology, Brigham and Women's Hospital.

[#] Department of Surgery, Brigham and Women's Hospital.

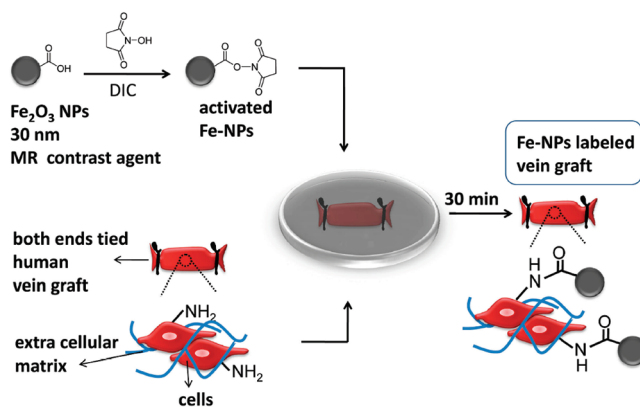


Figure 1. Schematic representation of the immobilization of Fe-NPs on human vein. Incubation of the vein in an activated Fe-NPs solution produces binding of Fe-NPs on its surface. Particles could bind to amine groups on the cell surface as well as the extracellular matrix.

conditions, and could potentially serve as a durable vein graft adventitial label to facilitate and enhance MR imaging.

Previously, we have demonstrated that *N*-hydroxysuccinamide esters of small target molecules could be covalently attached to amine groups that are present on the cell surface (17). Human mesenchymal stem cells modified through this method did not alter the inherent cell properties such as cell viability, proliferation, adhesion kinetics, and their stem cell phenotype. This suggests that covalent modification could be performed under conditions that have minimal impact on live cells. Thus, we adopted a similar strategy to covalently immobilize Fe-NPs on the surface of human veins. The current project capitalizes on the innovative synergy of commercially available Fe-NPs (modified to covalently bind to human tissue), and high spatial resolution MRI to enhance visualization of the entire vessel wall *ex vivo*. Specifically, we test the hypothesis that Fe-NPs can be covalently immobilized onto the external wall of human vein conduits and subsequently enable enhanced delineation of the adventitia through MR imaging.

Amine groups are present in abundance on the surface of various tissues (18) and are available to react with *N*-hydroxysuccinamide. After appropriate institutional approvals, freshly discarded human vein segments from bypass surgeries and major amputations were collected and “labeled” with commercially available Fe-NPs via a two-step reaction (Figure 1). Briefly, carboxylic groups that are on the magnetic nanoparticles’ surface were activated by reacting with *N*-hydroxysuccinamide esters. Subsequently, the activated particles were immediately used for coating the vein graft adventitia. With the luminal side protected via ligatures on either end, the test human vein sample was placed in a PBS filled Petri dish. The activated magnetic particles (in PBS) were added and incubated for 30 min at room temperature (for detailed synthesis methods, see Supporting Information). As a non-label control experiment, a vein segment was incubated in PBS (without Fe-NPs). Finally, all vein segments were individually and thoroughly rinsed thrice with PBS to remove unbound Fe-NPs. The current technique was applied with thirty minutes of incubation time, and this resulted in significant Fe-NP deposition on the vein; future optimization of the reaction conditions (e.g., pH, temperature) may accelerate this process.

Fe-NP labeled veins were thoroughly characterized using scanning electron microscopy (SEM) and energy dispersive X-ray analysis (EDAX). SEM images of labeled and unlabeled veins clearly show the presence of Fe-NPs on the surface of labeled veins (Figure 2). Results obtained from elemental mapping analysis (SEM-EDAX) show that Fe-NP coatings covered the majority of the labeled vein surface (Figure 3). In

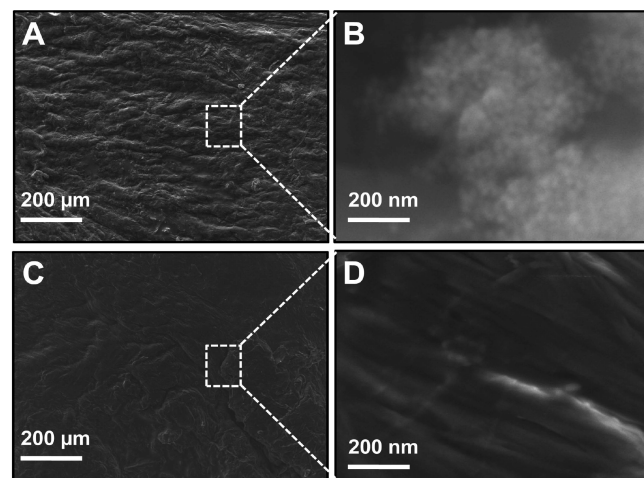


Figure 2. SEM images of the outer surface of the human veins with immobilized Fe-NPs (A and B) and without Fe-NPs (C and D).

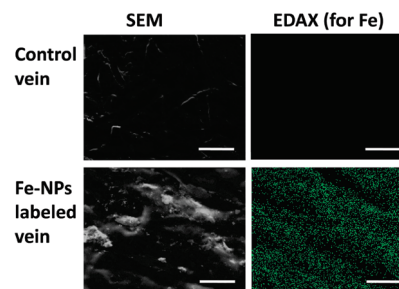


Figure 3. SEM micrograph (left) and Fe elemental mapping using EDAX (right) of unlabeled control (top row) and Fe-NPs labeled (bottom row) surface of the human veins. EDAX was positive (colored) for Fe on the Fe-NPs labeled portions only. In all images, scale bar represents 20 μm .

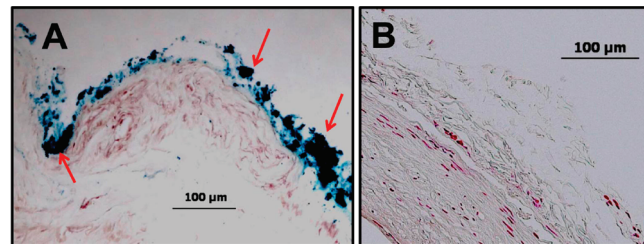


Figure 4. Iron histochemistry. Perl's Prussian blue staining images of (A) Fe-NPs labeled and (B) unlabeled human veins. Presence of Fe is confirmed by the appearance of dark blue/black colored areas (shown by red arrows in panel A).

addition, absence of Fe-NPs on the surface of unlabeled veins was confirmed (Figure 3). Iron histochemistry of labeled vein cross sections, using Perl's Prussian Blue protocol (see methods in Supporting Information), was also performed to visualize the location of Fe-NPs on the outer surface of the vein. Dark blue/black stains in the polarized microscopy images are attributed to the presence of Fe, suggesting that Fe is confined to the vein surface (Figure 4).

Prior to EDAX and histochemistry, MR imaging was employed to validate our strategy of utilizing the magnetic properties of Fe-NPs to readily delineate the vein surface from any surrounding MR signal-generating environment. Vein segments were immersed in saline to accomplish this task. Fe-NPs create a large dipolar magnetic field gradient that acts on the water molecules that diffuse close to the particles (19). They have a very large transverse to longitudinal relaxivity ratio, thus creating a predominant T_2^* effect resulting in MR signal

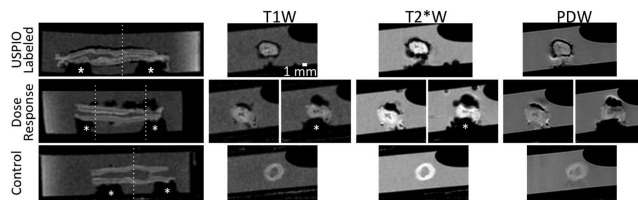


Figure 5. T1-weighted, T2*-weighted, and PD-weighted MR images ($0.3 \times 0.3 \times 0.5 \text{ mm}^3$ resolution) obtained at 3 T of three segments of the same saphenous vein: a segment circumferentially labeled with activated Fe-NPs as described in the text (top row); a segment with 4 equal drops of cyanoacrylate adhesive, each containing different concentration of Fe-NPs (middle row); the unlabeled control vein segment (bottom row). A sagittal curved multiplanar reformation of the T1W acquisition is shown in the first column; the dashed vertical lines indicate the locations of the axial images shown in the other columns. The concentration of Fe-NPs shown in the middle row of the sagittal reformation is 6, 12.5, 25, and 50 μg , from left to right. All vein segments were imaged immersed in Petri dishes filled with saline and mounted on polystyrene scaffolds (white stars in images) to suspend them within the fluid.

hypointensity (i.e., darker), as well as generating contrast in T1-, T2-, and T2*-weighted images (20).

T1-weighted (T1W), T2*-weighted (T2*W), and proton density-weighted (PDW) high-resolution (spatial resolution $0.3 \times 0.3 \times 0.5 \text{ mm}^3$) MR imaging of labeled and control vein specimens was performed on a clinical 3 T MRI scanner (HDX, General Electric, Milwaukee, WI) equipped with 40 mT/m gradients (150 T/m/s slew rate) (Figure 5). For detailed MRI methods, see Supporting Information. In addition, the MRI dose-response to different Fe-NPs concentrations was explored: four concentrations of Fe-NPs (50, 25, 12.5, and 6 μg) were each mixed with a drop of Cyanoacrylate adhesive and placed on the adventitia of an unlabeled vein prior to imaging. All three vein segments were imaged simultaneously (Figure 5). Additional experiments confirmed that Cyanoacrylate adhesive had no measurable effect for those image contrast weightings (not shown).

Quantitative assessment of the ability of the Fe-NPs to enhance delineation of the vein wall from surrounding signal was performed by direct planimetry of the vessel wall and surrounding signal voids caused by the Fe-NPs using region-of-interest (ROI) measurements; for detailed methods, see Supporting Information. In brief, three ROIs were drawn on each of the control and labeled samples in T1W images: a central ROI delineated the lumen, a second ROI delineated the outer extent of the vein-wall tissue, and a third ROI was used to delineate the region surrounding the vein. For the labeled vein, this encompassed the outer extent of the iron oxide susceptibility-induced signal void. In the control vein segment, this region was a similarly sized ROI containing some of the surrounding saline around the control specimen (Figure 6). ROI areas were used to deduce the average thickness of the vessel wall and surrounding Fe-NP label, as well as the relative signal characteristics of the vein wall tissue and label.

First, we tested the hypothesis that the vessel wall thickness could be accurately measured despite the presence of the iron oxide particles. The average wall thickness of the unlabeled control vein segment was $1.47 \pm 0.06 \text{ mm}$, while that of the labeled segment was $1.36 \pm 0.08 \text{ mm}$. The 0.11 mm difference in wall thickness was statistically significant (*t*-test, $p < 0.0001$). There were no apparent trends in wall thickness with slice location for either vein segment (Figure 7). Since both vein segments were obtained from consecutive portions of the same donor vein (1.5 cm length ea.), the observed difference in wall thickness was most likely due to the signal nulling effect of the Fe-NP on the labeled vein. This difference, however, is much

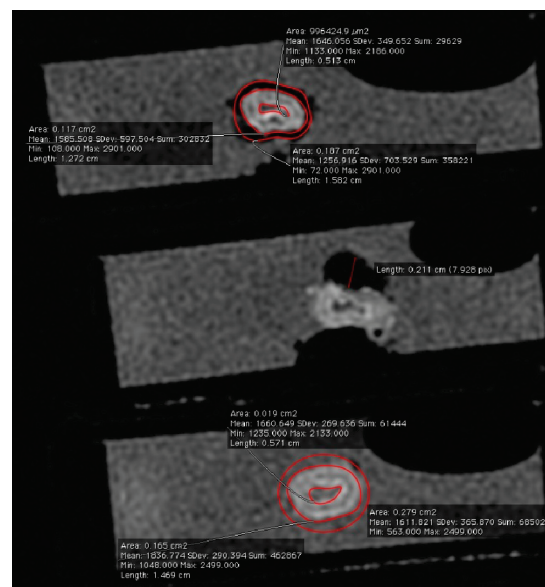


Figure 6. Definition of ROIs and lengths used for quantitative analyses; for each axial slice analyzed, a lumen ROI was first delineated for both the labeled and control segment. Next, a wall ROI was delineated for both segments. Finally, a third ROI extending to the edge of the Fe-NP label, or a corresponding similar region in the saline, was delineated for the labeled and control vein specimens, respectively. These ROIs were used to determine the average thickness of the vessel wall, the average thickness of the Fe-NP label, and the CNR between vessel wall and surrounding label or saline as appropriate. Finally, for the dose-response experiment, the maximal width of the signal void was measured for each axial slice along a line orthogonal to the vessel wall.

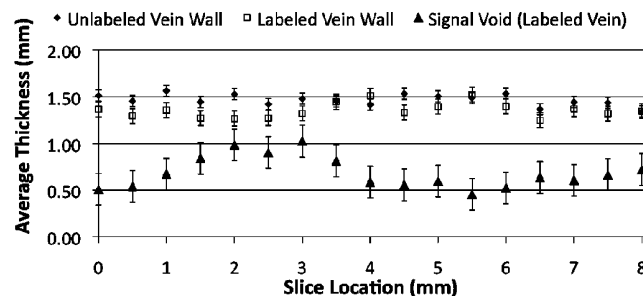


Figure 7. Average wall thickness of labeled and control vein segments in each slice analyzed along the length of the specimens, and average thickness of the iron-oxide susceptibility-induced signal void around the labeled vein. Error bars indicate the standard deviation of measurements across all slices.

lower than *in vivo* MR imaging resolutions and thus is unlikely to impact our ability to perform accurate wall thickness measurements. At present, the highest published resolution used for vein graft imaging is 0.312 mm in-plane (8–10), while most *in vivo* MRI is performed at resolutions higher than 0.5 mm due to scan time constraints at clinically used field strengths of 1.5–3 T.

A second analysis was performed to determine the ability of the Fe-NP label to enhance the delineation of the vessel wall boundary in comparison to the surrounding MR signal-generating environment. In general, this is a combination of the size of the structure to be delineated (e.g., Fe-NP label) compared to the image resolution, as well as the contrast to noise ratio of the structure (e.g., imposed between the wall tissue and the Fe-NP label).

For our *ex vivo* experiment, each of these two metrics was assessed separately. The average thickness of the Fe-NP label obtained from ROI measurements was $0.68 \pm 0.17 \text{ mm}$ (Figure

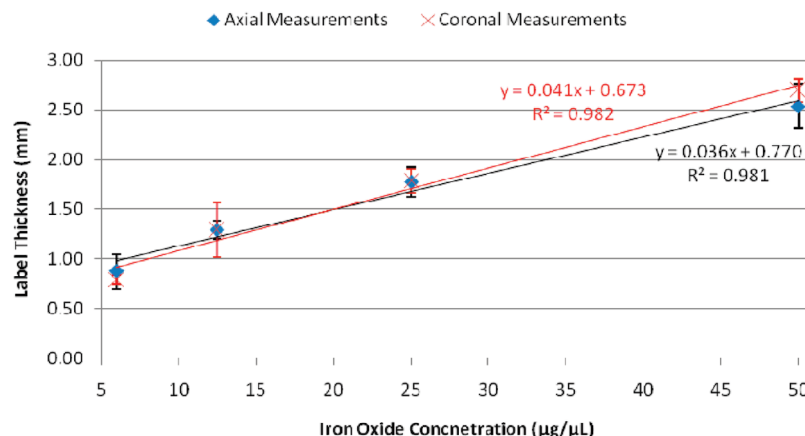


Figure 8. Correlation between label thickness and Fe-NP load observed in the dose–response experiment. Measurements were performed independently in both raw axial images, as well as coronal/sagittal multiplanar reformations.

7), well within the limits of in vivo MRI resolutions. In addition, the CNR between the vessel wall and surrounding label was 20.3 ± 2.4 . Such high CNR values observed with the Fe-NP label are uncommon in vessel wall MRI; the highest CNR values encountered are near 10, and represent signal differences between the vessel wall and the signal void within the lumen in black-blood MRI (21). CNRs are much lower between the vessel wall and surrounding signal-generating tissues for in vivo T1W vein graft imaging. Values near zero are often encountered when the vein wall is surrounded by muscle or scar tissues. Thus, the finding of this preliminary study is that the Fe-NP label produces an effect that is global (encompassing the entire vein wall irrespective of the surrounding signal) and that can be readily detected (high CNR) within the limitations of current in vivo MR imaging (extent greater than or equal to a single pixel).

While multiplanar reformation of the vein segment with the four concentrations of Fe-NP-loaded adhesive (50, 25, 12.5, and 6 μg) demonstrated a clear dose–response of the susceptibility-induced signal void (Figure 5), a final analysis was performed to determine the correlation between Fe-NP concentration and the thickness of the resulting label. As expected, there exists a strong linear relationship between the width of the Fe-NP susceptibility-induced signal void (Figure 6) and the iron oxide load of the cyanoacrylate adhesive (Figure 8). Careful control of the Fe-NP concentration will be critical, since at higher concentrations (above 12.5 μg), the signal void induced by the Fe-NPs interferes with visualization of the vein wall (Figure 5). Nonetheless, the linear response of the label to Fe-NP loading suggests that this adverse effect can be minimized by optimization of the reaction conditions to employ sufficiently low Fe-NP quantities with which to label the vein wall.

An interesting effect observed in this study is underscored by the “asymmetry” of the label thickness measurements in light of the wall thickness difference between labeled and control vein segments. Specifically, while the label measured nearly 0.7 mm thick, it only encroached 0.11 mm within the vessel wall. This anisotropic effect of the Fe-NPs (namely, the preferential nulling of signals outside the vessel wall rather than equally affecting the vein wall tissue signal) is likely explained by the increased mobility of the water protons in the saline compared to those in the vessel wall. As a result, we can postulate that in an in vivo environment the thickness of the label will likely be lower at the same concentration. Nonetheless, given current in vivo imaging resolutions and the large CNR attainable by the Fe-NP label developed in this work, this study suggests that sufficient label thicknesses (≥ 0.3 mm) can be readily achieved to delineate the label without affecting measurement of the vein wall tissue.

Data obtained from our ex vivo studies highlight the potential application of Fe-NPs to enhance vein graft wall visualization in vivo. By enhancing the sensitivity of MRIs to clearly delineate the entire vessel wall, the relationship between vein wall remodeling and early events (first four weeks post implantation) may eventually be investigated longitudinally and more efficiently. Such studies to date have required invasive imaging techniques. External wall labeling with Fe-NPs may serve to enhance the sensitivity of MRI by helping to more readily delineate the vessel adventitia; this would be potentially useful in the in vivo setting, where improving cranial caudal coverage within clinical scan time remains a challenge. Since negative wall remodeling (permanent constriction of the vein graft) stands as an important etiology of failure (3–6), more sensitive delineation of early negative remodeling may also enable timely clinical interventions to halt the process.

The vein conduit labeling techniques can be expanded to include other contrast agents such as gadolinium metal complexes that can provide enhanced graft wall MR signals, thus further improving the efficacy and resolution of MRI as a tool to investigate vein grafts (and other solid organ surfaces). On the basis of these promising ex vivo results, we are in the process of evaluating the stability and toxicity of this agent and strategy using in vivo animal models. The potential long-term effects of Fe-NPs localization on the surface of vein grafts, as well as other distant organs such as liver and kidneys will be investigated. The present strategy may also be combined with molecular/biologically based contrast agents to provide a better understanding of vascular wall remodeling mechanisms and improve our understanding of vein graft failure.

ACKNOWLEDGMENT

The authors would like to thank Prof. Frederick J. Schoen, M.D., Ph.D., and Dr. Sivapriya Kirubakaran for helpful discussions. J.M.K. acknowledges American Heart Association grant #0970178N and NIH R01HL095722 for financial support. P.K.V. would like to thank the Ewing Marion Kauffman Foundation for Entrepreneur Postdoc Fellowship. C.K.O. acknowledges NIH grant #1R01HL079135 and 5T32HL007734-16 for financial support.

Supporting Information Available: Detailed materials and methods. This material is available free of charge via the Internet at <http://pubs.acs.org>.

LITERATURE CITED

- (1) Conte, M. S., Bandyk, D. F., Clowes, A. W., Moneta, G. L., Seely, L., Lorenz, T. J., Namini, H., Hamdan, A. D., Roddy,

- S. P., Belkin, M., Berceli, S. A., DeMasi, R. J., Samson, R. H., and Berman, S. S. (2006) Results of PREVENT III: a multicenter, randomized trial of edifoligide for the prevention of vein graft failure in lower extremity bypass surgery. *J. Vasc. Surg.* **43**, 742–751, discussion 751.
- (2) Alexander, J. H., Hafley, G., Harrington, R. A., Peterson, E. D., Ferguson, T. B., Jr., Lorenz, T. J., Goyal, A., Gibson, M., Mack, M. J., Gennevois, D., Califf, R. M., and Kouchoukos, N. T. (2005) Efficacy and safety of edifoligide, an E2F transcription factor decoy, for prevention of vein graft failure following coronary artery bypass graft surgery: PREVENT IV: a randomized controlled trial. *JAMA* **294**, 2446–2454.
- (3) Lau, G. T., Ridley, L. J., Bannon, P. G., Wong, L. A., Trieu, J., Brieger, D. B., Lowe, H. C., Freedman, B. S., and Kritharides, L. (2006) Lumen loss in the first year in saphenous vein grafts is predominantly a result of negative remodeling of the whole vessel rather than a result of changes in wall thickness. *Circulation* **114**, I435–40.
- (4) Owens, C. D. (2009) Adaptive changes in autogenous vein grafts for arterial reconstruction: Clinical implications. *J. Vasc. Surg.*
- (5) Wu, J., and Zhang, C. (2009) Neointimal hyperplasia, vein graft remodeling, and long-term patency. *Am. J. Physiol.* **297**, H1194–5.
- (6) Jiang, Z., Tao, M., Omalley, K. A., Wang, D., Ozaki, C. K., and Berceli, S. A. (2009) Established neointimal hyperplasia in vein grafts expands via TGF-beta-mediated progressive fibrosis. *Am. J. Physiol.* **297**, H1200–7.
- (7) Yuan, C., and Kerwin, W. S. (2004) MRI of atherosclerosis. *J. Magn. Reson. Imaging* **19**, 710–9.
- (8) Mitsouras, D., Mulkern, R. V., Owens, C. D., Conte, M. S., Ersoy, H., Luu, T. M., Whitmore, A. G., Creager, M. A., and Rybicki, F. J. (2008) High-resolution peripheral vein bypass graft wall studies using high sampling efficiency inner volume 3D FSE. *Magn. Reson. Med.* **59**, 650–4.
- (9) Crowe, L. A., Gatehouse, P., Yang, G. Z., Mohiaddin, R. H., Varghese, A., Charrier, C., Keegan, J., and Firmin, D. N. (2003) Volume-selective 3D turbo spin echo imaging for vascular wall imaging and distensibility measurement. *J. Magn. Reson. Imaging* **17**, 572–80.
- (10) Koktzoglou, I., Chung, Y. C., Carroll, T. J., Simonetti, O. P., Morasch, M. D., and Li, D. (2007) Three-dimensional black-blood MR imaging of carotid arteries with segmented steady-state free precession: initial experience. *Radiology* **243**, 220–8.
- (11) Bulte, J. W., Zhang, S., van Gelderen, P., Herynek, V., Jordan, E. K., Duncan, I. D., and Frank, J. A. (1999) Neurotransplantation of magnetically labeled oligodendrocyte progenitors: magnetic resonance tracking of cell migration and myelination. *Proc. Natl. Acad. Sci. U.S.A.* **96**, 15256–61.
- (12) Josephson, L., Tung, C. H., Moore, A., and Weissleder, R. (1999) High-efficiency intracellular magnetic labeling with novel superparamagnetic-Tat peptide conjugates. *Bioconjugate Chem.* **10**, 186–91.
- (13) Lee, H., Lee, E., Kim do, K., Jang, N. K., Jeong, Y. Y., and Jon, S. (2006) Antibiofouling polymer-coated superparamagnetic iron oxide nanoparticles as potential magnetic resonance contrast agents for in vivo cancer imaging. *J. Am. Chem. Soc.* **128**, 7383–9.
- (14) McCarthy, J. R., and Weissleder, R. (2008) Multifunctional magnetic nanoparticles for targeted imaging and therapy. *Adv. Drug Delivery Rev.* **60**, 1241–51.
- (15) Weissleder, R., Kelly, K., Sun, E. Y., Shtatland, T., and Josephson, L. (2005) Cell-specific targeting of nanoparticles by multivalent attachment of small molecules. *Nat. Biotechnol.* **23**, 1418–23.
- (16) Gupta, A. K., Naregalkar, R. R., Vaidya, V. D., and Gupta, M. (2007) Recent advances on surface engineering of magnetic iron oxide nanoparticles and their biomedical applications. *Nanomed. (London, England)* **2**, 23–39.
- (17) Sarkar, D., Vemula, P. K., Teo, G. S., Spelke, D., Karnik, R., Wee le, Y., and Karp, J. M. (2008) Chemical engineering of mesenchymal stem cells to induce a cell rolling response. *Bioconjugate Chem.* **19**, 2105–9.
- (18) Artzi, N., Shazly, T., Baker, A. B., Bon, A., and Edelman, E. R. (2009) Aldehyde-amine chemistry enables modulated biosealants with tissue-specific adhesion. *Adv. Mater.* **21**, 3399–3403.
- (19) Winter, P. M., Caruthers, S. D., Yu, X., Song, S. K., Chen, J., Miller, B., Bulte, J. W., Robertson, J. D., Gaffney, P. J., Wickline, S. A., and Lanza, G. M. (2003) Improved molecular imaging contrast agent for detection of human thrombus. *Magn. Reson. Med.* **50**, 411–6.
- (20) Tang, T. Y., Muller, K. H., Graves, M. J., Li, Z. Y., Walsh, S. R., Young, V., Sadat, U., Howarth, S. P., and Gillard, J. H. (2009) Iron oxide particles for atheroma imaging. *Arterioscler. Thromb. Vasc. Biol.* **29**, 1001–8.
- (21) Balu, N., Chu, B., Hatsukami, T. S., Yuan, C., and Yarnykh, V. L. (2008) Comparison between 2D and 3D high-resolution black-blood techniques for carotid artery wall imaging in clinically significant atherosclerosis. *J. Magn. Reson. Imaging* **27**, 918–24.

BC100138C